Journal of Atmospheric and Solar–Terrestrial Physics 220 (2021) 105650

Contents lists available at ScienceDirect

Journal of Atmospheric and Solar-Terrestrial Physics

journal homepage: www.elsevier.com/locate/jastp

Trends in the polar summer mesosphere temperature and pressure altitude from satellite observations

Scott M. Bailey [a,*], Brentha Thurairajah [a], Mark E. Hervig [b], David E. Siskind [c], James M. Russell III [d], Larry L. Gordley [e]

[a] Center for Space Science and Engineering Research, Bradley Department of Electrical and Computer Engineering, Virginia Tech, Blacksburg, VA, USA
[b] GATS Inc, Driggs, ID, USA
[c] Naval Research Laboratory, Washington, DC, USA
[d] Center for Atmospheric Science, Hampton University, Hampton, VA, USA
[e] GATS Inc, Newport News, VA, USA

ARTICLE INFO

Keywords:
Mesosphere
Temperature
Trends

ABSTRACT

Time series of mesospheric temperature and pressure altitude are produced through combining observations by the Halogen Occultation Experiment (HALOE), Sounding of the Atmosphere Using Broadband Emission Radiometry (SABER), and Solar Occultation for Ice Experiment (SOFIE) instruments. Time series of both temperature and pressure altitude are produced through the combination of HALOE/SABER providing 29 years in length and HALOE/SOFIE providing 22 years in length. The different sampling of the three instruments constrains the time series to June in the northern hemisphere and December in the southern hemisphere and 64–70° in both hemispheres. We interpret the time series by fitting them to simple descriptions of the variations including solar, intra-hemispheric, inter-hemispheric, and linear trend terms. The inferred intra- and inter-hemispheric terms show that dynamical influences rival solar variability in the mesosphere. We find a robust result that the mesosphere is in general cooling at most altitudes at approximately 1–2 K per decade in response to greenhouse gas increases. That cooling leads to a shrinking of the atmosphere on the order of 100–200 m per decade. The shrinking leads to a reduction in cooling and eventually a warming near 0.005 hPa due to hydrostatic contraction.

1. Introduction

Trends or long-term changes typically refer to changes in atmospheric parameters over a decade or more. Modelling and observational studies regarding the mesosphere have suggested that the observed trends in upper atmospheric parameters are due to the increase in greenhouse gas concentration, like carbon dioxide (CO_2) (Roble and Dickinson (1989); Rishbeth and Roble (1992), Laštovička and Pancheva (1991); Laštovička, 2013 and 2017; Lübken et al., 2020). For example, Qian et al. (2017) used observations from the Atmospheric Chemistry Experiment-Fourier Transform Spectrometer (ACE-FTS) (Bernath et al., 2005) on board the Canadian SCISAT-1 satellite and the Sounding of the Atmosphere using Broadband Emission Radiometry (SABER) instrument onboard the Thermosphere Ionosphere Mesosphere Energetics Dynamics (TIMED) satellite to show that the CO_2 trend is increasing in the upper mesosphere by ~5% per decade. While increases in greenhouse gases are considered the main reason for the increase in surface temperature, in the upper atmosphere increases in these gases cause cooling. This is because the upper atmosphere is optically thin to outgoing longwave energy and will therefore radiate more energy, leading to more efficient cooling.

Several studies have confirmed this cooling or negative trend in the mesosphere (Laštovička, 2017 and references therein) including recent lidar (Yuan et al., 2019), satellite (Zhao et al., 2020; Li et al., 2020), and modelling (Qian et al., 2019) studies. For example, Yuan et al. (2019) used annual mean lidar temperature observations from 1990 to 2018 at mid-latitudes (~41°N) and reported a cooling trend of more than 2 K/decade near the mesopause. Zhao et al. (2020) used annual mean SABER mesopause temperatures from 2002 to 2019 to detect a cooling trend varying of ~0 to - 0.14 K/decade at all latitudes. Li et al. (2020) used merged Halogen Occultation Experiment (HALOE) and SABER observations between 1991 and 2018 and found significant cooling

* Corresponding author. 450 Whittemore Hall, Virginia Tech, Blacksburg, VA, 2460, USA.
E-mail address: baileys@vt.edu (S.M. Bailey).

https://doi.org/10.1016/j.jastp.2021.105650
Received 1 December 2020; Received in revised form 2 April 2021; Accepted 8 April 2021
Available online 20 April 2021

trends over 45°S to 45°N latitude and 40–80 km altitude, with a maximum value of ~1.2 K/decade near 60–70 km. Qian et al. (2019) used global WACCM-X model simulations and radar measurements of winds from mid-latitudes (51°N) during 1980–2014 to find an average cooling of ~ -1K/decade in the middle to lower mesosphere. The Yuan et al. and Zhao et al. observational studies also reported a negative trend in the mesopause height. With regard to the geometric heights of mesospheric pressure levels, model studies (Akmaev et al., 2006; Lübken et al. 2009, 2013; Lübken and Berger, 2011) indicate a shrinking of the height of the mesosphere attributed to greenhouse gas cooling. This hydrostatic contraction lowers the height of mesospheric pressure levels and leads to cooling just below PMC heights and warming just above (e.g. Lübken and Berger, 2011; Lübken et al., 2013). We know of no observational studies to date of trends in mesospheric pressure heights, but Friedrich et al. (2017) have suggested such trends based on studies of observed D and E-region electron densities.

Long-term trends in the high-latitude summer mesosphere have been studied using Polar mesospheric cloud (PMC) observations (DeLand and Thomas, 2015; Hervig et al., 2016a; Dalin et al., 2020; Lübken et al., 2020 and references therein). PMCs are ice clouds that are usually observed in the high-latitude summer mesosphere (~82–86 km) when temperatures are low (<~145K). More recently these clouds are becoming more visible at mid-latitudes (e.g. Hervig et al., 2016b) and low-latitudes (Russell et al., 2014). Changes in both temperature and water vapor (H_2O) are equally important in causing PMCs to vary. Hervig et al. (2016a) analyzed 36 years of PMC data measured by the SBUV instrument revealing that temperatures are decreasing by 0.5 ± 0.2 K per decade and H_2O is increasing by 0.07 ± 0.03 ppmv per decade. On a long-term basis, at high-latitudes PMCs have been found to respond to a variety of parameters including the 11-year solar cycle (Hervig et al., 2016b) and greenhouse gases (Lübken et al., 2020). Hervig et al. (2019) reported an apparent dramatic response of PMCs to the 11-year solar cycle in the 1980s and 1990s, that is absent in the 2000s. Lübken et al. (2020) used 138 years of LIMA model simulations and reported prominent trends in mesospheric ice layers after the 1960s when the increase in CO_2 and H_2O accelerated. Other parameters such as space traffic (Stevens et al., 2012) and ozone (Dalin et al., 2020) have also been reported to have an influence on PMC variability.

On a short-term basis, PMCs and the summer mesospheric temperatures also respond to atmospheric wave dynamics such as planetary waves (e.g. France et al., 2018), tides (e.g. Stevens et al., 2017), and gravity waves (e.g. Dalin et al., 2016; Thurairajah et al., 2020). Atmospheric dynamics are responsible for intra-hemispheric and inter-hemispheric coupling that have been shown to influence PMC variability (e.g. Gumbel and Karlsson, 2011). Intra-hemispheric coupling denotes the dynamical influence of the lower atmosphere on the summer mesosphere, in the same hemisphere. Inter-hemispheric coupling refers to the dynamical influence of the lower atmosphere in the winter hemisphere on the summer mesosphere. Although atmospheric dynamics have been shown to have a major influence on the upper atmospheric temperature on short time scales, very few studies exist on the long-term trends in atmospheric dynamics. In a review of progress in upper atmospheric trends, Laštovička (2017) identified the lack of studies on long-term trend in atmospheric circulation and wave activity as a key problem in our understanding of the long-term upper atmospheric trends. A few studies exist on trends in winds and associated atmospheric dynamics and gravity waves (e.g. Jacobi et al., 2012; Liu et al., 2017; Qian et al., 2019). For example, Jacobi et al. (2012) used radar data and noted that zonal wind trends showed the influence of planetary wave trends, Liu et al. (2017) used satellite data and found significant linear trends in gravity wave potential energy, and Qian et al. (2019) used model simulations that showed that wind trends and solar cycle effects on these winds were predominantly controlled by atmospheric dynamics.

In this study we combine data from the HALOE (1991–2005), SABER (2002–2020) instruments, and the Solar Occultation for Ice Experiment (SOFIE; 2007–2012) instrument to analyze the long-term mesospheric temperature and geometric altitude trend in the high-latitude summer mesosphere of both hemispheres. While Zhao et al. (2020) did report on the annual mean linear and solar temperature trends using SABER, they did not show the linear trends in the summer, because of the yaw cycle of the TIMED satellite that allows for only ~2-months of high-latitude summer observations. Also, as mentioned above, Li et al. (2020) only examined trends in the low to mid-latitudes. In our study, by combining HALOE and SABER observations we use an extended satellite record (i.e. 29 years) to investigate the solar cycle and linear trends in temperature and geometric altitude in the high-latitude summer. We also investigate the effect of inter- and intra-hemispheric coupling on these trends to understand the dynamical influence of the lower atmosphere. We also perform an identical analysis on time series formed by combining HALOE and SOFIE. Although combined HALOE and SOFIE observations provide a shorter time series, 22 years, SOFIE observations offer higher fidelity altitude registration. Thus the second time series offers increased information and mutual validation of results obtained from both.

2. Datasets

HALOE conducted solar occultation measurements from the Upper Atmosphere Research Satellite (UARS). (Russell et al., 1993). HALOE collected profiles of middle atmospheric composition, pressure, and temperature from September 1991 to November 2005. In the mesosphere, temperatures were retrieved from the 2.8 μm CO_2 channel transmission measurement (Gordley et al., 2009a). Validation of HALOE temperature retrievals can be found in Hervig et al. (1996) and Remsberg et al. (2002). For this study we use the HALOE V19 temperature and pressure data. These data are available at a vertical resolution of ~2.3 km with a vertical sampling interval of 0.3 km.

SABER on the TIMED satellite measures vertical profiles of pressure, temperature, and trace species (Russell et al., 1999) using infrared emission observations. SABER data are available from January 2002 and measurements are ongoing. SABER temperatures are retrieved from the limb radiance in the 15 μm CO_2 band and have been validated by Remsberg (2008). Data are available at a vertical resolution of ~2 km with a vertical sampling interval of 0.4 km. We use the version 2.0 dataset.

SOFIE conducts solar occultation measurements from the Aeronomy of Ice in the Mesosphere (AIM) satellite to characterize vertical profiles of temperature, pressure, trace gases, and PMC properties (Gordley et al., 2009b). Temperatures are retrieved from atmospheric transmission in the 4.3 μm CO_2 band and atmospheric refraction at 701 nm (Marshall et al., 2011). Validation of the SOFIE temperatures can be found in Stevens et al. (2012) and Hervig et al. (2016b). Data are available at a vertical resolution of ~1.6 km with a vertical sampling interval of 0.2 km. This work used Version 1.3 data.

To be consistent across all datasets we use zonal mean monthly averaged data from the latitude band 64–70° during June in the Northern Hemisphere (NH) and December in the Southern Hemisphere (SH). Figs. 1 and 2 show the latitude coverage for each instrument as a function of day in June and December, respectively. While SOFIE data are available daily at these latitudes during the months of June and December, SABER did not make observations during the last few days in June and December in years 2018, 2019, 2020. This is because of the SABER yaw cycle, and the fact that the end days of high-latitude observations have progressively shifted to earlier in the summer with increasing years. For example, in 2002 SABER observed latitudes poleward of ~50°N from 22 May – 16 July. In 2020, SABER observed these latitudes from 28 April to 23 June. Since we use monthly averages, this earlier end date for these few years does not present a problem in the analysis. HALOE data however, are available less frequently poleward of 45°. To address this data gap, and obtain monthly means we fit to available HALOE data using SOFIE points as anchors from 1 May to 30 August. The fits to the data are then used to calculate the required

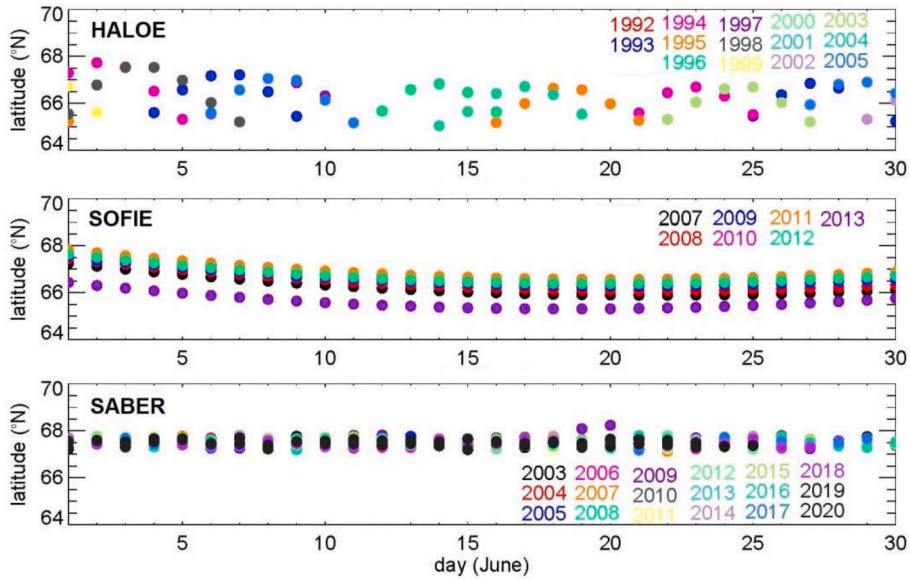

Fig. 1. Latitude coverage between 64 and 70°N observed by HALOE (1992–2005), SOFIE (2007–2012) and SABER (2003–2020) in June.

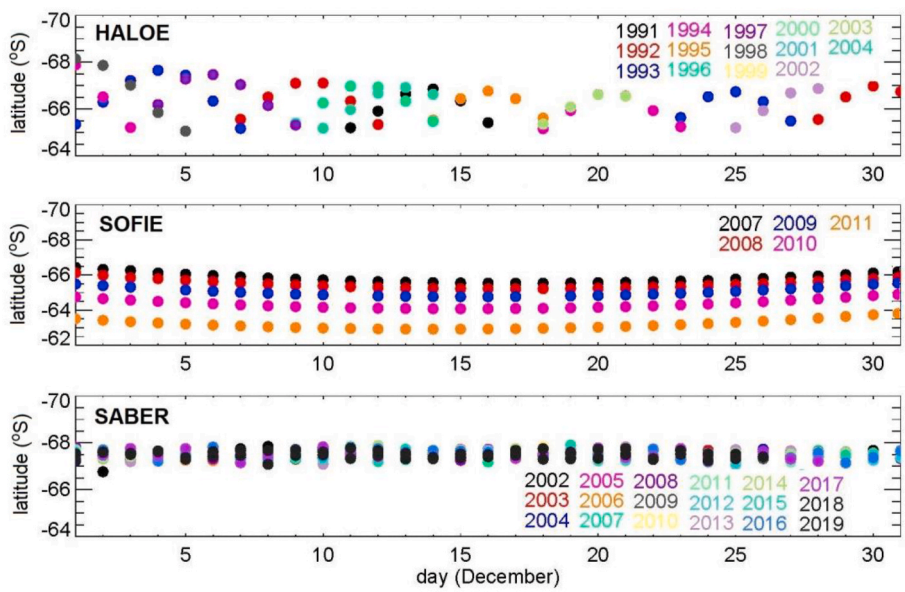

Fig. 2. Latitude coverage between 64 and 70°S observed by HALOE (1991–2004), SOFIE (2007–2009) and SABER (2002–2019) in December. SOFIE observes latitudes close to 63N in year 2011, and the y-axis is shown from 62 to 70°S.

monthly means. The fitting method was successfully demonstrated by Hervig and Siskind (2006) without the benefit of SOFIE data. Using SOFIE in the current application to improve the fits is appropriate since SOFIE and HALOE are both solar occultation instruments with similar retrieval techniques and measurement geometry.

To be consistent across altitudes, all data are binned on constant pressure levels from 1.0 to 0.001 hPa (~50–95 km). Figs. 3 and 4 show the HALOE, SABER, SOFIE temperature and altitude at 0.01 hPa for the NH and SH, respectively. The error bars for SOFIE and SABER are calculated as the 1-sigma standard deviation in the averages. To determine the HALOE uncertainties, fits were performed to SOFIE data using HALOE sampling, and the resulting errors were taken as uncertainties in the HALOE fits. HALOE observations were also corrected for biases in temperature and altitude relative to SABER for years when the two missions overlapped. Combining HALOE and SABER observations provides 29 years of data in both hemispheres i.e. June of 1992–2020 in NH and December of 1991–2019 in SH. There is overlap during 2003–2005 in the NH and 2002–2004 in the SH. For our study we used the average value from HALOE and SABER. HALOE/SOFIE observations provide 22 years of data in the NH from 1992 to 2013 (including a data gap in 2006) and 21 years in the SH from 1991 to 2011 (including a data gap in 2005 and 2006). Figs. 3 and 4 include the correction and show that the overlapping data are generally in agreement within the mutual uncertainties of the observations.

For all three datasets, retrievals are performed on geometric altitude as the vertical scale. Pressure is determined from observed CO_2 transmission (emission for SABER) and these pressures are registered in altitude through matching with those from meteorological reanalysis at the lower altitudes (Beaver et al., 1994; Russell et al., 1999; Marshall et al., 2011).

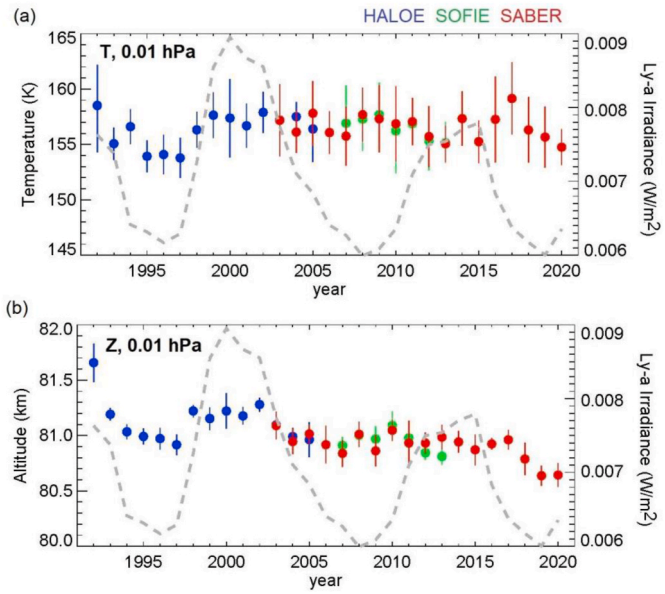

Fig. 3. Zonal mean monthly June (a) temperature and (b) altitude at 0.01 hPa and averaged over 65–70°N from HALOE (blue), SOFIE (green), and SABER (red). The solar Lyman alpha irradiance is also shown (grey dashed line).

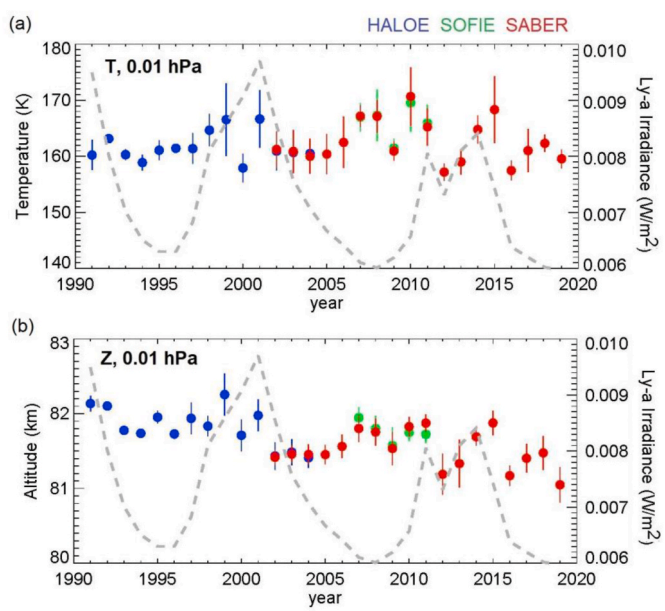

Fig. 4. Same as Fig. 3 but December and averaged over 65–70°S.

3. Method

In order to understand and interpret the temperature and pressure altitude time series, they are described using multiple regression to a set of terms that represent variations due to solar, inter-hemispheric and intra-hemispheric coupling, a linear trend, and an autocorrelation term. The regression model is expressed as:

$$T(p_i) = A_0 + A_{solar}(p_i)\cdot Ind_{Ly\alpha} + A_{\text{intra}}(p_i)\cdot Ind_{\text{intra}} + A_{\text{inter}}(p_i)\cdot Ind_{\text{inter}} + A_{linear}(p_i)^* t_i + A_{auto}(p_i)^* t_{i-1} \quad (1)$$

In equation (1), A represents the coefficients for various terms as labeled. They are functions of pressure level i, p_i. Ind represents the indices used to represent the various processes. A_0 is the constant term, representing the mean of the time series. Lyman-alpha data are available as the integration of the solar irradiance over 121–122 nm (Machol et al., 2019). The intra and inter-hemispheric indices are calculated as described below from the National Center for Environmental Prediction/National Center for Atmospheric Research (NCEP/NCAR) daily global dataset available at a spatial resolution of 2.5° latitude x 2.5° longitude from 1000 to 10 mb. $T(p_i)$ is the satellite temperature variation at pressure level p_i. An identical equation is used to describe variations in the observed pressure altitudes. The mean temperature and pressure altitude are subtracted from the observations so that the model is used only to describe variations.

To calculate the intra-hemispheric and inter-hemispheric indices, the NCEP temperature data is averaged over 100-10 hPa (~15–30 km). For the intra-hemispheric term, temperatures are averaged over 65–70°N for the NH and 65-70°S for the SH. The range of average temperatures in the NH is 228.8–230.8 K. The range of temperatures in the SH is 232.4–238.2 K. The greater range values in the SH reflect the interannual variability in summer season onset as the Antarctic ozone hole breakup can sometimes be delayed in very late SH spring (Karlsson et al., 2011).

For the inter-hemispheric term, temperatures are averaged over 40-60°S for the NH and 60–80°N for the SH. Using these latitudes as the basis for an inter-hemispheric index is based on the study by Gumbel and Karlsson (2011) who found that the PMC occurrence correlated with stratospheric temperatures in the same hemisphere (intra) and opposite hemisphere (inter) at these latitude and altitude ranges. For our time series, the range of SH temperatures used in the NH index is 210.0–214.7 K. The range of NH temperatures used in the SH index is 203.7–214.7 K.

The Lyman-alpha irradiance, intra- and inter-hemispheric temperatures are averaged over June (NH) and December (SH). The monthly averaged inter-hemispheric temperature is shifted by −7 days (e. g. November 23 to December 23 in the NH) to account for the lag in inter-hemispheric coupling (Gumbel and Karlsson, 2011) effect. The solar effect (11-year variability) on the intra- and inter-hemispheric terms are removed. This effect is small and we have verified that none of the results of this paper are changed in any significant way if this step is not done. All three index data sets are de-trended by a linear fit and are normalized to unity amplitude.

Equation (1) and the associated indices comprise a very simplified description of the observed variability. Such simplicity is warranted given the limited number of data points in the time series, but should be sufficient to yield insight concerning the relative importance of the drivers of the variations and in particular the magnitude of the linear trends. Month-long bins are driven primarily by the HALOE sampling. Some dynamical effects occur on shorter time scales; however, the more significant of such events, Sudden Stratospheric Warmings, occur primarily in winter, while we focus in this work on summer. We therefore conclude that using month-long bins does not significantly impact the results of our approach.

Figs. 5 and 6 show the temperature and pressure altitude at 0.01 hPa and the multiple regression fit to the data for the NH and SH, respectively. The de-trended and normalized intra-hemispheric and inter-hemispheric terms are also shown. The magnitude of each of these terms is then calculated by using a non-linear least squares fitting method or the Levenberg - Marquardt model (Press et al., 1992) to find a best fit to the time series. Uncertainties in the fit parameters are calculated from the resulting covariance matrix.

4. Results

To understand the relative importance of each term, we first perform the regression to temperature and pressure altitude for only the linear, solar, and autocorrelation terms. The coefficients are calculated from both the extended satellite record combining HALOE/SABER, and HALOE/SOFIE datasets. Tables 1 and 2 (first two rows) list coefficient results at key pressure levels. Autocorrelation results are not included as

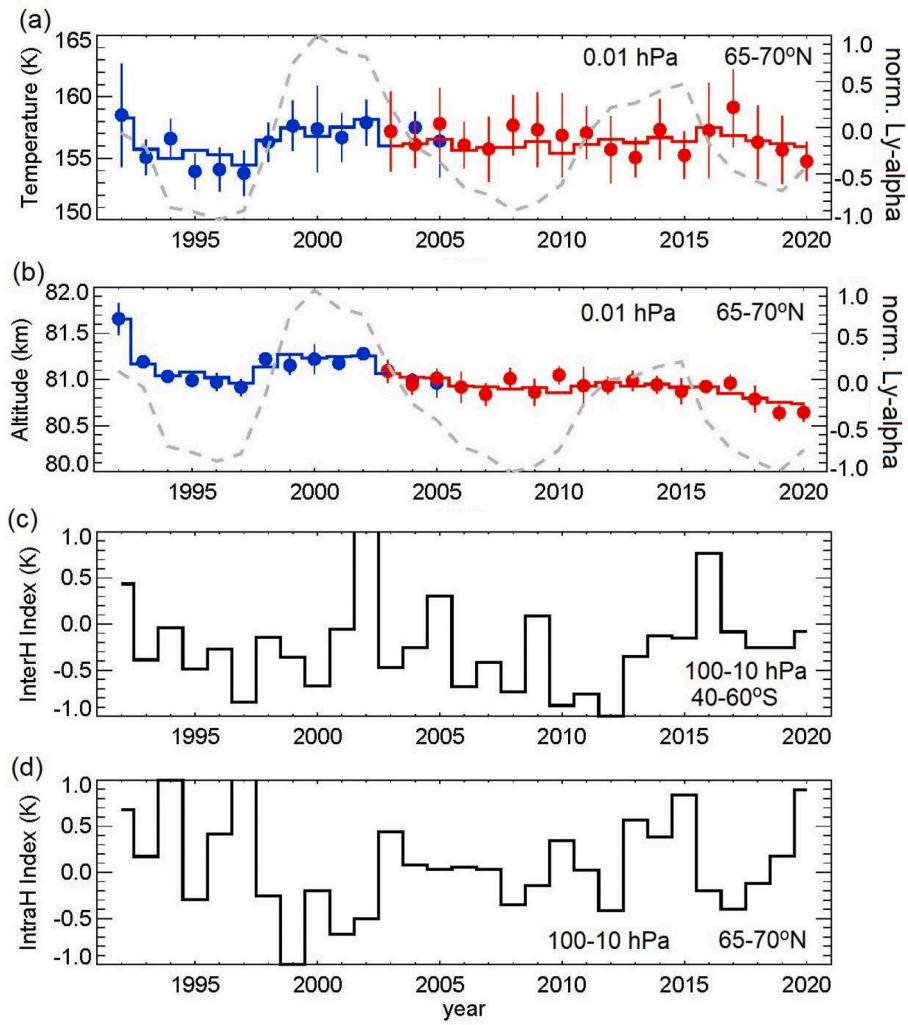

Fig. 5. Non-linear least squares fit to NH HALOE (blue) and SABER (red) (a) temperatures and (b) altitude at 0.01 hPa. The Lyman-alpha irradiance (grey dashed line) is also shown. (c) De-trended normalized inter-hemispheric index (d) De-trended normalized intra-hemispheric index.

they were found to be negligible. Fig. 7 shows the retrieved terms for both temperature and pressure altitude plotted as a function of pressure level from 1.0 to 0.001 hPa (~50–95 km) for both the NH and SH. The results from the two data sets (HALOE/SABER and HALOE/SOFIE) are very similar and, in many cases, nearly identical. Significant differences are found only in the SH linear term, though the general features of the profile are similar in both.

In both hemispheres, the solar influence on temperature is mostly positive, with some negative or zero response in the SH. The agreement between the two datasets suggests a robustness to the interpretation of the times series. The small differences between the two can be attributed to the difference in the lengths of the datasets. For the linear trend in temperatures, both hemispheres show 1–2 K per decade trend that decreases with decreasing pressure until ~0.02 (NH) to 0.06 (SH) hPa where the trend reduces and becomes a warming peaking at around 0.004 hPa in both hemispheres. The temperature trend just below PMC heights (i.e. below ~0.01 hPa; ~84 km) is cooling, but at this height the cooling trend crosses zero and turns to warming at higher altitudes. The solar effect on pressure altitude is positive at all pressure levels studied and increases with decreasing pressure. The linear trends in the pressure altitude are negative at all altitudes. The trend slightly decreases with height in both hemispheres until about 0.01 hPa, above which the trend is reduced.

To understand the quality of the fits, Fig. 8 shows χ^2 results for each of the fits as a function of pressure level. The χ^2 values are defined as:

$$\chi^2 = \frac{1}{\upsilon}\sum_i \frac{(T_m(p_i) - T(p_i))^2}{\sigma_i^2} \tag{2}$$

where $T_m(p_i)$ is the model temperature at pressure p_i based on the indices and coefficients found at that pressure level; σ_i is the uncertainty in the observed temperature at pressure p_i; and υ is the number of degrees of freedom defined as the number of observations in the time series minus the number of fitted parameters. A similar equation is used for pressure altitudes.

Results for the solar and linear term model described above show relatively large values of χ^2 for temperature peaking near 0.1 hPa in both hemispheres, suggesting that the two-term description is too simple to represent the datasets well. Fig. 8 also shows χ^2 results for models including an intra-hemispheric term and both intra- and inter-hemispheric terms. For temperature in both hemispheres, the introduction of the dynamics terms significantly improves the fits, although in the SH the addition of the inter-hemispheric term does not significantly improve the fits and much of the high χ^2 values peaking near 0.1 hPa remain. In the case of pressure altitude, the introduction of the dynamics terms has a smaller impact overall and primarily play a role at low pressures in the NH and higher pressures in the SH. In both hemispheres the χ^2 values increase with decreasing pressure. The χ^2 values are lower for the pressure altitude time series than for the temperature below ~0.01 hPa, and the reverse is true above that level.

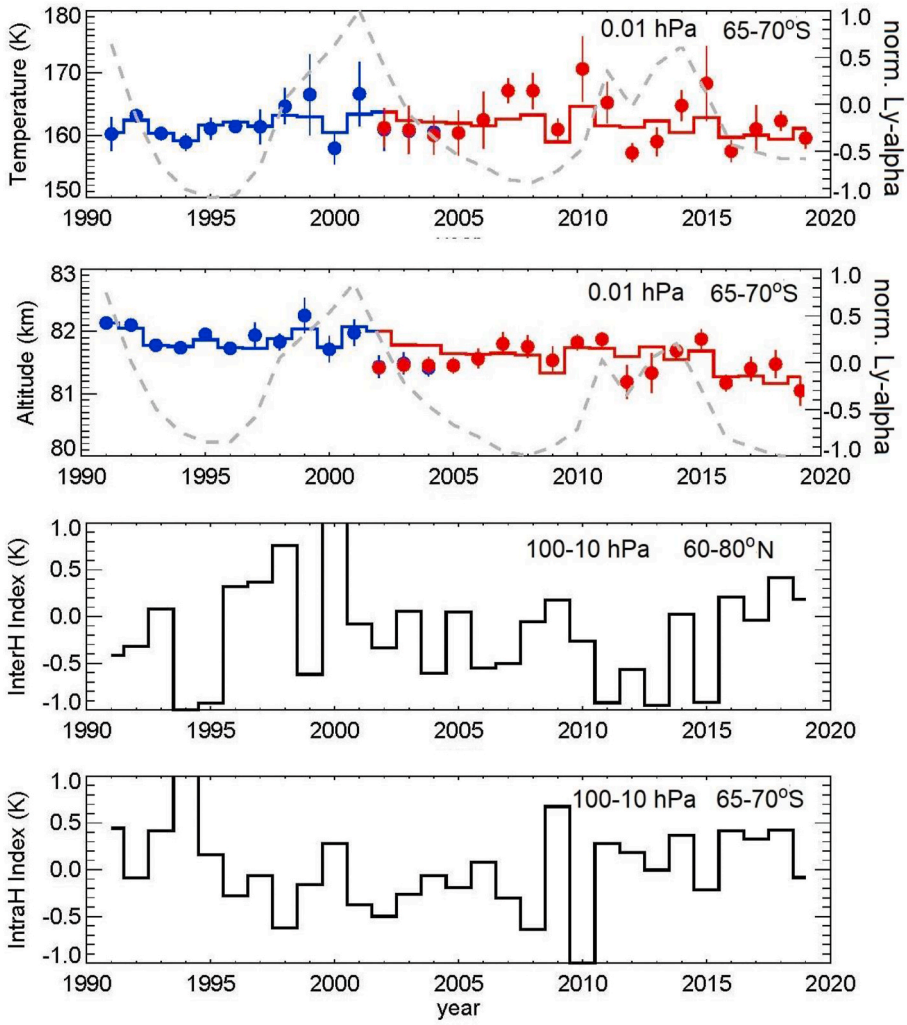

Fig. 6. Same as Fig. 5 but for the SH.

Table 1
Solar and linear temperature terms.

Before adding coupling (intra- and inter- hemispheric) terms				
T	NH		SH	
	0.1 hPa	0.005 hPa	0.1 hPa	0.005 hPa
Solar (K)	1.2 ± 0.2	0.7 ± 0.7	0.07 ± 0.21	1.0 ± 0.7
Linear (K/decade)	−1.0 ± 0.2	2.2 ± 0.5	−1.9 ± 0.2	1.1 ± 0.3
After adding coupling terms				
Solar (K)	0.1 ± 0.3	1.5 ± 1.0	−0.9 ± 0.3	1.2 ± 0.7
Linear (K/decade)	−0.9 ± 0.2	1.8 ± 0.5	−1.8 ± 0.2	0.9 ± 0.4

Table 2
Solar and linear altitude terms.

Before adding coupling (intra- and inter- hemispheric) terms				
Z	NH		SH	
	0.1 hPa	0.005 hPa	0.1 hPa	0.005 hPa
Solar (m)	89.6 ± 36.7	202.9 ± 21.0	100.9 ± 55.0	185.1 ± 37.9
Linear (m/decade)	−84.6 ± 32.2	−90.9 ± 17.1	−152.0 ± 28.6	−122.3 ± 27.5
After adding coupling terms				
Solar (m)	88.8 ± 57.1	173.4 ± 33.3	106.3 ± 55.2	117.9 ± 43.1
Linear (m/decade)	−97.1 ± 31.3	−132.2 ± 17.7	−137.6 ± 30.6	−205.1 ± 31.7

Figs. 9 and 10 shows the regression results for including all of the terms in Equation (1). Tables 1 and 2 (last two rows) provide results of the linear and solar terms at specific pressure levels after adding the coupling terms. Autocorrelation terms are again found to have only negligible effect. The largest autocorrelation term found was 0.05 K for temperature and at most pressure levels less than 0.01 K, while for pressure altitude the largest term was about 5 m and often smaller. Autocorrelation terms are not discussed further. As in Fig. 7, there is little difference in the results from the two time series, except for the SH linear pressure-altitude term, again suggesting robustness in the interpretation.

The solar term in the NH temperature shows a peak near 0.003 hPa in both hemispheres with the term approaching zero near 0.002 hPa. In the NH, the term remains small at higher pressures. In the SH, a negative peak near 0.04 hPa is found. The intra-hemispheric term in temperature shows some sign of a peak near 0.004 hPa in both hemispheres, with a slightly larger magnitude in the NH. At higher pressures a strong negative peak is found in both hemispheres near 0.04 hPa. By 1.0 hPa in both hemispheres this term approaches zero. The inter-hemispheric terms in temperature are positive at all pressures in the NH, but only significantly positive near 0.01 hPa in the SH. In the NH the inter-hemispheric terms are on average near 1 K in amplitude and generally decrease with height. The linear term in temperature shows a strong

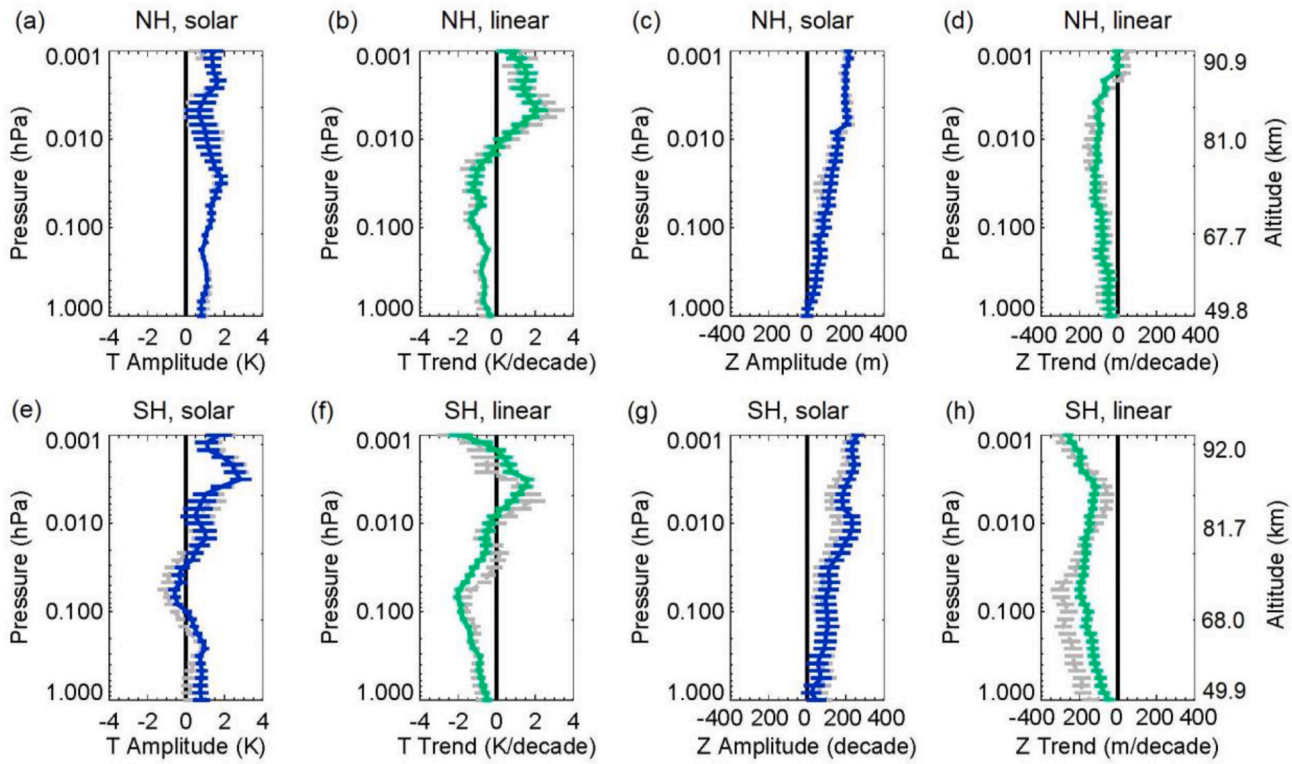

Fig. 7. (Upper panel) Solar (blue) and linear (green) trends in (a, b) temperature and (c, d) altitude from HALOE/SABER in the NH. Grey lines indicate trends from HALOE/SOFIE. (lower panel) Same as upper panel but for the SH trends in (e, f) temperature and (g, h) altitude.

positive peak near 0.005 hPa in both hemispheres, though stronger in the NH. A negative peak appears in the NH near 0.03 hPa and in the SH near 0.05 hPa. In both hemispheres the term approaches zero near 1 hPa.

Pressure altitude solar terms are positive at all pressure levels and generally increase with decreasing pressure. The NH term shows a stronger increase above 0.01 hPa reaching 250 m at 0.001 hPa (Figs. 9 and 10). The intra-hemispheric terms in altitude are positive near 1.0 hPa and decrease with altitude crossing zero at 0.2 hPa in the NH and 0.03 hPa in the SH. In both hemispheres there is a minimum value of about −150 m near 0.01 hPa which increases to near zero at 0.001 hPa. The inter-hemispheric term in altitude is approximately −100 m near 1.0 hPa and increases with little structure to approximately 150 hPa in the NH. In the SH this term is roughly constant from 1.0 to 0.001 hPa at approximately 150 hPa. The linear trends in pressure altitude are negative at all altitudes in both hemispheres. In the NH the trend decreases with height in both hemispheres until about 0.01 hPa, above which the trend is reduced and reaches to nearly zero at 0.001 hPa. In the SH the change in slope is seen slightly in the HALOE/SOFIE results, but not in the HALO/SABER results.

5. Discussion

Due to the lack of long-term observations of the mesosphere (other than HALOE prior to 2002), the only source of validation for this period is from models. Qian et al. (2019) used model simulations to study solar effects and linear trends in the mesosphere as a function of month, latitude, and altitude. For the solar term, in the SH December they found a value of 5 K per solar flux unit (SFU) near 85 km. This value converts to approximately 2.5 K for comparison to the present approach, which is in agreement with Fig. 9. They also found a negative solar influence near 70 km, as reported here, although the Qian et al. magnitude was about −1 K compared to our −2 K. In the NH June, Qian et al. found a weaker solar effect compared to that described above for the SH, whereas we show a similar magnitude at the peak and little or no negative affect near 70 km. Given the complexities of the comparison and the fact that Qian et al. did not isolate solar effects from intra- and inter-hemispheric coupling, we find the agreement acceptable.

Intra-hemispheric coupling in the summer upper atmosphere has been studied in detail by Siskind et al. (2003; 2005) and Coy et al. (2005) using simulations and comparison to SABER observations. Our results of mesospheric cooling in response to stratospheric warming, with peak magnitude between 0.1 and 0.01 hPa, are in excellent agreement with their results. Siskind et al. (2005) and Coy et al. (2005) focus on winter and find the coupling controlled by planetary waves. Siskind et al. (2003) focus on summer and find the coupling to be controlled by gravity waves and their filtering by stratospheric winds. In the upper mesosphere our results show, in agreement with both Siskind et al. and Coy et al., a temperature increase following a stratospheric temperature increase. This heating may be hydrostatic contraction in response to the dynamical influences.

Inter-hemispheric coupling at PMC altitudes has been studied by Karlsson et al. (2009), Siskind et al. (2011), Gumbel and Karlsson (2011). The connection arises from gravity wave impacts on stratospheric winds and associated changes in the global mesospheric circulation. They used the same inter-hemispheric index as used here and found that an increase in the index led to a warming and subsequent reduction in PMCs. A warming at PMC heights agrees with the present work. Karlsson and Becker (2016) further explored inter-hemispheric coupling and found that inter-hemispheric effects play a constant role, rather than simply event driven one, in the mesosphere. Our results support that conclusion. The present results suggest that the larger temperature variability in the NH winter does not lead to larger impacts of inter-hemispheric coupling in the SH for the latitude and month we are studying. This result may be consistent with Karlsson et al. and Siskind et al. who show that the effects of inter-hemispheric coupling have strong latitudinal and altitude dependencies. . Additionally, the differing PMC altitudes in the two hemispheres (Bailey et al., 2007)

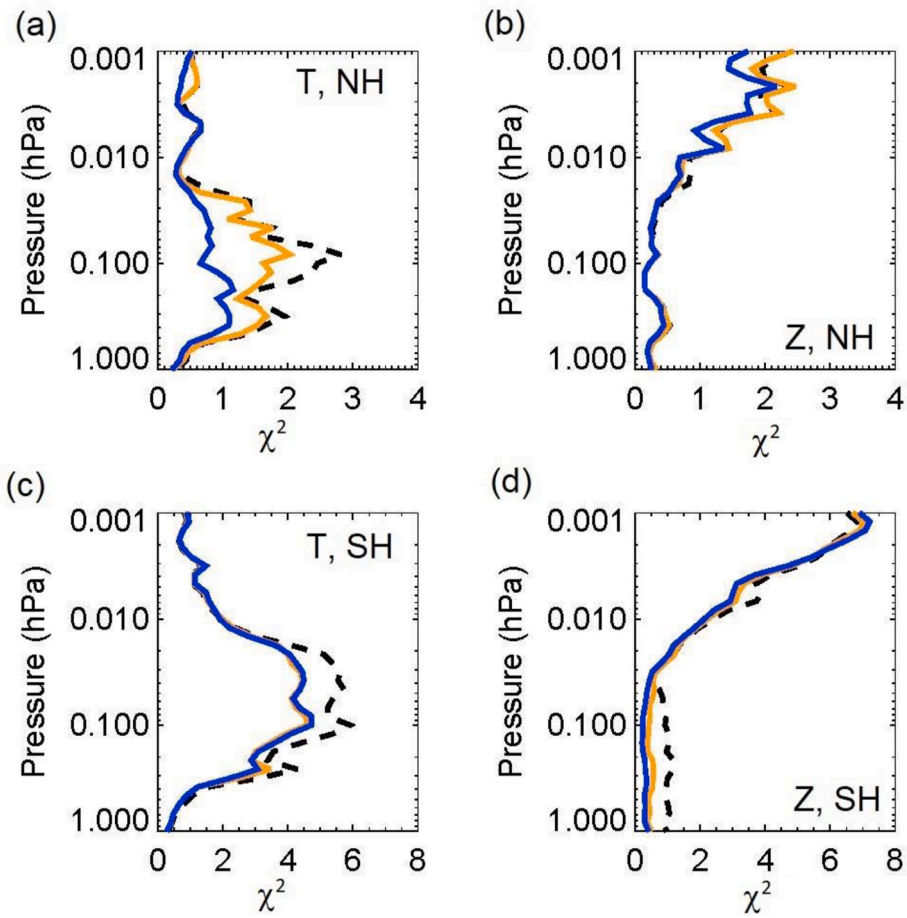

Fig. 8. The reduced χ^2 fit to solar and linear terms (dashed line), solar, linear, and intra-hemispheric term (orange) and solar, linear, inter, and intra hemispheric terms (blue) for the temperature and geometric altitude fits in the NH and SH. All fits include the auto correlation term.

suggests that inter-hemispheric coupling can project differently in each. Further research is needed on this topic. The most significant intra-hemispheric trends in temperature are negative while the inter-hemispheric trends are positive. The addition of the coupling terms increases the positive solar effects in the upper mesosphere while the dynamics terms decrease and even become zero near PMC heights. The linear trends are not affected by the addition of the coupling terms. The fact that the inclusion of the dynamics terms changed the solar term results significantly highlights that dynamical influences are as important in the mesosphere as solar variability.

Given the limited number of samples in the time series and the very simplified description of the complex physics provided by the two dynamics indices, we feel the general agreement with expected behavior is very good and strengthens our results for the linear trend. A longer time series will allow for a more sophisticated treatment.

Qian et al. found a linear trend of about −1 to −2 K per decade in both SH December and NH June in the middle mesosphere, with a slightly stronger trend in the SH, in agreement with the present work. They also found a strong positive trend of about 1.5 K per decade in the December SH upper mesosphere and near zero in the June NH. The present work shows a stronger positive peak in the NH compared to the SH, but the SH magnitudes are comparable. Given the variability with month and latitude in the Qian results, the agreement is taken as acceptable.

Akmaev et al. (2006) and more recently Lübken et al. (2013) performed model studies examining temperature trends in the mid-latitude mesosphere. Lübken et al. examined the relative roles of radiative cooling by CO_2 and O_3. The present results cannot resolve the source of the observed cooling so we compare to their combined results which showed mesospheric trends of −1 to −1.8 K/decade for the period 1960–2008. They found that the temperature trends peaked at 70–75 km. While the present results are for only the later years, the two results are in good agreement concerning the magnitude and height dependence in the trends. Both the observations and the model results approach zero above the altitude of peak cooling, with the observations crossing into a warming above 0.01 hPa, near approximately 83 km. The observed heating is due to hydrostatic contraction of the atmosphere at higher altitudes as suggested by both Akmaev et al. and Lübken et al.

In general, increases (with altitude) in the regression terms for temperature result in increasing regression terms for pressure altitudes in our results. This shows that the temperature and pressure altitude results are in qualitative agreement, which is important since the two are derived from very different techniques and assumptions. We see a reduction in shrinking where the temperature trend is peaked, in agreement with the temperature results showing a conversion from cooling to heating.

The NH turn in the pressure altitude trend (less cooling above 0.02 hPa) is at the same altitude where the temperature trend also changes slope (Fig. 9). This is consistent with the observed change from a cooling trend to a warming trend near the PMC altitudes. The slope is fairly constant in the SH, with a slight turn only in the HALOE/SOFIE time series. The pressure altitude results here are in good agreement with Lübken et al. (2013) both in shape and magnitude, even though their results are for midlatitudes. This is particularly true for the SH as Lübken et al. show only a small turn toward a lower trend at higher altitudes. The linear trend decreasing with altitude shows that the inferred shrinking is primarily occurring in the mesosphere itself, and not due to shrinking of the stratosphere. Cooling of the mesosphere by increased

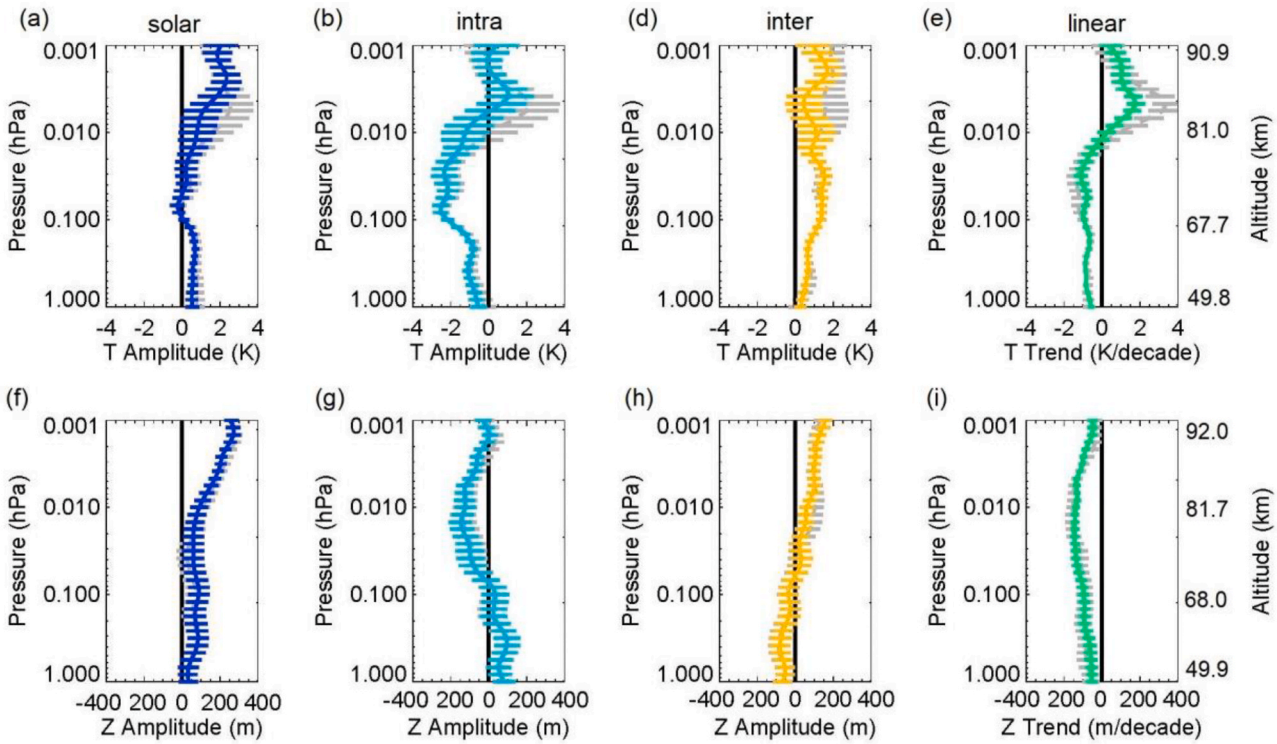

Fig. 9. NH (upper panel) Temperature trends and (lower panel) Altitude trends from HALOE and SABER in the NH. Grey lines indicate trends from HALOE and SOFIE.

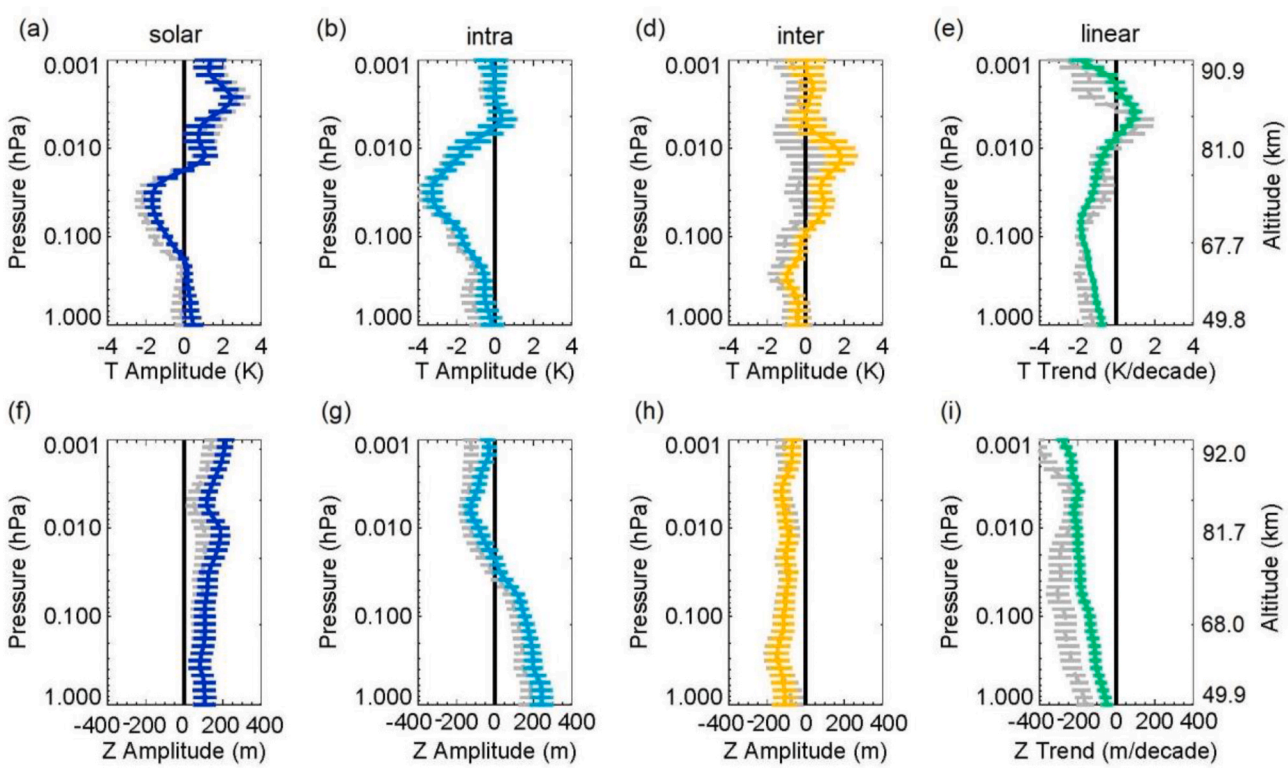

Fig. 10. Same as Fig. 9 but for the SH.

greenhouse gases explain this as demonstrated by Lübken et al. We believe this to be the first observational confirmation of the mesosphere shrinking. While we utilize a simplified description of the atmosphere (Equation (1)) to interpret our temperature and pressure altitude time series, this result is robust and changes little depending on whether the HALOE/SABER or HALOE/SOFIE time series is used or the dynamics

terms are included or not.

Our results show that near the altitudes of PMC formation, the temperature trend changes from cooling to warming. This reversal in trends is curious in that an increasing trend in PMCs is evident in both the long-term PMC observations (Hervig et al., 2019; DeLand and Thomas, 2019) and in PMC models (e.g., Berger and Lübken, 2015; Lübken et al., 2020), which would be consistent with at least a small cooling trend (Hervig et al., 2016b). Understanding trends in PMCs is useful due to their extreme sensitivity to their environment and to dynamical influences. The altitude resolution of the present results and the uncertainties in the analysis make it difficult to determine whether our results are consistent with observed PMC trends. This will be a subject of future research. Recent work has shown that PMC changes are not currently consistent with the solar cycle (Hervig et al., 2019). The present results suggest that the lack of solar cycle response is due to low solar activity and the resulting dominance of dynamical effects.

6. Summary and conclusions

We have created time series of NH and SH polar summer mesospheric temperature and pressure altitude from observations by the HALOE, SABER, and SOFIE satellite instruments. Due to the sampling of the three instruments, the time series are constructed only for June in the NH and December in the SH and latitudes of ~64–70° in both hemispheres. The HALOE/SABER time series is 29 years in length and the HALOE/SOFIE time series is 22 years in length. Using a simplified description of the variability including terms for solar, intra-hemispheric, and inter-hemispheric variations, we were able to isolate linear trends in both temperature and pressure altitude throughout the mesosphere. The inferred intra-hemispheric and inter-hemispheric terms are consistent with previous work and show that dynamical influences rival solar variability in the mesosphere. The linear term in temperature shows a negative peak in the NH near 0.03 hPa and in the SH near 0.05 hPa. In both hemispheres there is a strong positive peak near 0.005 hPa, though stronger in the NH. In both hemispheres the term approaches zero near 1 hPa. The linear trends in pressure altitude are negative at all altitudes in both hemispheres. These results are consistent with a mesosphere that is cooling at most altitudes at approximately 1–2 K per decade in response to greenhouse gas increases. That cooling leads to a shrinking of the atmosphere. The shrinking leads to a reduction in cooling and eventually a warming due to hydrostatic contraction. This warming occurs just above the altitude at which PMCs form, suggesting that PMCs form at an altitude of small temperature trends. These results present the first observational confirmation of a shrinking mesosphere. The rate of the shrinking is approximately 150–200 m per decade throughout much of the mesosphere. These results can be improved upon with more observations, which should be possible as the SABER and SOFIE missions continue. Future work will include analysis of mid-latitudes using HALOE and SABER.

This work highlights the richness and complexity of the mesopause region. With the formation of PMCs and their extreme sensitivity to environment, the importance of inter-hemispheric coupling, and both intra-hemispheric coupling and long-term trends changing from negative to positive effects all within a small region of altitude, this region remains an important and interesting topic of study.]

Declaration of competing interest

The authors declare that they have no known competing financial interests or personal relationships that could have appeared to influence the work reported in this paper.

Acknowledgments

We thank the HALOE, SABER, and SOFIE teams for the observations and the AIM science team for helpful discussions. HALOE, SABER, and SOFIE data are available at http://haloe.gats-usa.net/download/index.php, http://saber.gats-usa.net/data_services.php, and http://sofie.gats-usa.net/sofie/index.php respectively. This work was supported by NASA's small explorer program.

References

Akmaev, R.A., Fomichev, V.I., Zhu, X., 2006. Impact of middle-atmospheric composition changes on greenhouse cooling in the upper atmosphere. J. Atmos. Sol. Terr. Phys. https://doi.org/10.1016/j.jastp.2006.03.008.

Bailey, S.M., Merkel, A.W., Thomas, G.E., Rusch, D.W., 2007. Hemispheric differences in polar mesospheric cloud morphology observed by the student nitric oxide explorer. J. Atmos. Sol. Terr. Phys. 69, 1407–1418. https://doi.org/10.1016/j.jastp.2007.02.008.

Beaver, G.M., Gordley, L.L., Russell III, J.M., 1994. Halogen Occultation Experiment (HALOE) altitude registration of atmospheric profile measurements: lessons learned and improvements made during the data validation phase. Proc. SPIE 2266, Optical Spectroscopic Techniques and Instrumentation for Atmospheric and Space Research. https://doi.org/10.1117/12.187564, 30 September 1994.

Berger, U., Lübken, F.-J., 2015. Trends in mesospheric ice layers in the Northern Hemisphere during 1961-2013. J. Geophys. Res. 120, 11. https://doi.org/10.1002/2015JD023355, 277–11,298.

Bernath, P.F., McElroy, C.T., Abrams, M.C., Boone, C.D., Butler, M., Camy-Peyret, C., Carleer, M., Clerbaux, C., Coheur, P.-F., Colin, R., DeCola, P., De Maziere, M., Drummond, J.R., Dufour, D., Evans, W.F.J., Fast, H., 2005. Atmospheric Chemistry experiment (ACE): mission overview. Geophys. Res. Lett. 32, L15S01. https://doi.org/10.1029/2005GL022386.

Coy, L., Siskind, D.E., Eckermann, S.D., PeMcCormack, J., Allen, D.R., Hogan, T.F., 2005. Modeling the August 2002 minor warming event. Geophys. Res. Lett. 32 https://doi.org/10.1029/2005GL022400. L07808.

Dalin, P., et al., 2016. A case study of long gravity wave crests in noctilucent clouds and their origin in the upper tropospheric jet stream. J. Geophys. Res. Atmos. 121, 14. https://doi.org/10.1002/2016JD025422, 102– 14,116.

Dalin, P., Perminov, V., Pertsev, N., Romejko, V., 2020. Updated long-term trends in mesopause temperature, airglow emissions, and noctilucent clouds. J. Geophys. Res.: Atmospheres 124. https://doi.org/10.1029/2019JD030814.

DeLand, M.T., Thomas, G.E., 2015. Updated PMC trends derived from SBUV data. J. Geophys. Res. Atmos. 120, 2140–2166. https://doi.org/10.1002/2014JD022253.

DeLand, M.T., Thomas, G.E., 2019. Extending the SBUV PMC data record with OMPS NP. Atmos. Chem. Phys. Discuss. https://doi.org/10.5194/acp-2018-1034.

France, J.A., Randall, C.E., Lieberman, R.S., Harvey, V.L., Siskind, D.E., Lumpe, J., Bailey, S.M., Carstens, J., Eckermann, S.D., Russell III, J.M., 2018. Local and remote planetary wave effects on polar mesospheric clouds in the Northern Hemisphere in 2014. J. Geophys. Res.: Atmospheres 123, 5149–5162. https://doi.org/10.1029/2017JD028224.

Friedrich, M., Pock, C., Torkar, K., 2017. Long-term trends in the D- and E-region based on rocket-borne measurements. J. Atmos. Sol. Terr. Phys. https://doi.org/10.1016/j.jastp.2017.04.009.

Gordley, L.L., Thompson, E., McHugh, M., Remsberg, E., Russell III, J., Magill, B., 2009a. Accuracy of atmospheric trends inferred from the Halogen Occultation Experiment (HALOE) data. J. Appl. Remote Sens. 3, 33526 doi:10.1117/1.3131722.

Gordley, L.L., et al., 2009b. The solar occultation for ice experiment. J. Atmos. Sol. Terr. Phys. 71, 300–315. https://doi.org/10.1016/j.jastp.2008.07.012.

Gumbel, J., Karlsson, B., 2011. Intra- and inter-hemispheric coupling effects on the polar summer mesosphere. Geophys. Res. Lett. 38, L14804 doi:10.1029/2011GL047968.

Hervig, M.E., Siskind, D.E., 2006. Decadal and inter-hemispheric variability in polar mesospheric clouds, water vapor, and temperature. J. Atmos. Sol. Terr. Phys. https://doi.org/10.1016/j.jastp.2005.08.010.

Hervig, M.E., et al., 1996. Validation of temperature measurements from the halogen occultation experiment. J. Geophys. Res. 101, 285, 10,277–10.

Hervig, M.E., Berger, U., Siskind, D.E., 2016a. Decadal variability in PMCs and implications for changing temperature and water vapor in the upper mesosphere. J. Geophys. Res. 121, 2383–2392. https://doi.org/10.1002/2015JD024439.

Hervig, M.E., Gerding, M., Stevens, M.H., Stockwell, R., Bailey, S.M., Russell, J.M., Stober, G., 2016b. Mid-latitude mesospheric clouds and their environment from SOFIE observations. J. Atmos. Sol. Terr. Phys. https://doi.org/10.1016/j.jastp.2016.09.004.

Hervig, M.E., Siskind, D.E., Bailey, S.M., DeLand, Russell III., J.M., Merkel, A., 2019. The missing solar cycle response of the polar summer mesosphere". Geophys. Res. Lett. https://doi.org/10.1029/2019GL083485.

Jacobi, C., Hoffmann, P., Liu, R.Q., Merzlyakov, E.G., Portnyagin, Yu.I., Manson, A.H., Meek, C.E., 2012. Long-term trends, their changes, and interannual variability of Northern Hemisphere midlatitude MLT winds. J. Atmos. Sol.-Terr. Phys. 75–76, 81–91. https://doi.org/10.1016/j.jastp.2011.03.016.

Karlsson, B., Randall, C.E., Benze, S., Mills, M., Harvey, V.L., Bailey, S.M., RussellIII, J. M., 2009. Intra-season alvariability of polarmesospheric clouds due to inter-hemispheric coupling. Geophys. Res. Lett. 36, L20802. https://doi.org/10.1029/2009GL040348.

Karlsson, B., Randall, C.E., Shepard, T.G., Lumpe, J., Nielson, K., Bailey, S.M., Hervig, M. E., Russell, J.M., 2011. On the seasonal onset of polar mesospheric clouds and the breakdown of the stratospheric polar vortex in the southern hemisphere. J. Geophys. Res. 116. D18107doi: 2011JD015989.

Karlsson, B., Becker, E., 2016. How does interhemispheric coupling contribute to cool down the summer polar mesosphere? J. Climate 29, 8807–8821. https://doi.org/10.1175/JCLI-D-16-0231.1.

Laštovička, J., 2013. Trends in the upper atmosphere and ionosphere: recent progress. J. Geophys. Res. Space Phys. 118, 3924–3935. https://doi.org/10.1002/jgra.50341.

Laštovička, J., Pancheva, D., 1991. Changes in characteristics of planetary waves at 80–100 km over central and southern europe since 1980. Adv. Space Res. 11 (3), 31–34.

Laštovička, J., 2017. A review of recent progress and trends in the upper atmosphere. J. Atmos. Sol. Terr. Phys. 163, 2–13. https://doi.org/10.1016/j.jastp.2017.03.009, 2017.

Liu, X., Yue, J., Xu, J., Garcia, R.R., Russell, J.M., Mlynczak, M., Wu, D.L., Nakamura, T., 2017. Variations of global gravity waves derived from 14 years of SABER temperature observations. J. Geophys. Res. Atmos. 122, 6231–6249. https://doi.org/10.1002/2017JD026604.

Li, T., Yue, J.M., Russell III, Zhang, X., 2020. Long-term trend and solar cycle in the middle atmosphere temperature revealed from merged HALOE and SABER datasets. J. Atmos. Sol. Terr. Phys. (in press).

Lübken, F.-J., Berger, U., 2011. Latitudinal and interhemispheric variation of stratospheric effects on mesospheric ice layer trends. J. Geophys. Res. 116, D00P03. https://doi.org/10.1029/2010JD015258.

Lübken, F.-J., Berger, U., Baumgarten, G., 2013. Temperature trends in the midlatitude summer mesosphere. J. Geophys. Res. Atmos. 118, 360. https://doi.org/10.1002/2013JD020576, 13,347–13.

Lübken, F.-J., Baumgarten, G., Berger, 2020. U., Long term trends of mesospheric ice layers: a model study. J. Atmos. Sol. Terr. Phys. https://doi.org/10.1016/j.jastp.2020.105378.

Machol, J., Snow, M., Woodraska, D., Woods, T., Viereck, R., Coddington, O., 2019. An improved lyman-alpha composite. Earth Space Sci. 6, 2263–2272. https://doi.org/10.1029/2019EA000648.

Marshall, B.T., Deaver, L.E., Thompson, R.E., Gordley, L.L., McHugh, M.J., Hervig, M.E., Russell III, J.M., 2011. Retrieval of temperature and pressure using broadband solar occultation: SOFIE approach and results. Atmos. Meas. Tech. 4, 893–907. https://doi.org/10.5194/amt-4-893-2011.

Press, W.H., Teukolsky, S.A., Vetterling, W.T., Flannery, B.P., 1992. Numerical Recipes in FORTRAN, the Art of Scientific Computing. Cambridge Univ. Press, New York, p. 965.

Qian, L., Burns, A.G., Solomon, S.C., Wang, W., 2017. Carbon dioxide trends in the mesosphere and lower thermosphere. J. Geophys. Res. Space Phys. 122, 4474–4488. https://doi.org/10.1002/2016JA023825.

Qian, L., Jacobi, C., McInerney, J., 2019. Trends and solar irradiance effects in the mesosphere. J. Geophys. Res.: Space Phys. 124, 1343–1360. https://doi.org/10.1029/2018JA026367.

Remsberg, E., et al., 2002. An assessment of the quality of Halogen Occulation Experiment temperature profiles in the mesosphere based on comparisons with Rayleigh backscatter lidar and inflatable falling sphere measurements. J. Geophys. Res. 107 https://doi.org/10.1029/2001JD001521.

Remsberg, et al., 2008. Assessment of the quality of the Version 1.07 temperature versus-pressure profiles of the middle atmosphere from TIMED/SABER. JGR 113. https://doi.org/10.1029/2008JD010013. D17101.

Rishbeth, H., Roble, R.G., 1992. Cooling of the upper atmosphere by enhanced greenhouse gases – modeling of thermospheric and ionospheric effects. Planet. Space Sci. 1011–1026, 40.

Roble, R.G., Dickinson, R.E., 1989. How will changes in carbon dioxide and methane modify the mean structure of the mesosphere and lower thermosphere? Geophys. Res. Lett. 16, 1441–1444.

Russell III, J.M., Mlynczak, M.G., Gordley, L.L., Tansock, J., Esplin, R., 1999. An overview of the SABER experiment and preliminary calibration results. Denver, Colo. In: Proceedings of the SPIE, 44th Annual Meeting, vol. 3756, pp. 277–288, 18–23 July.

Russell III, James M., Park, Larry L. Gordley Jae H., Roland Drayson, S., Donald Hesketh, W., Cicerone, Ralph J., Tuck, Adrian F., Frederick, John E., Harries, John E., Crutzen, Paul J., 1993. The halogen occultation experiment. J. Geophys. Res. Atmospheres. https://doi.org/10.1029/93JD00799.

Russell, J.M., Rong, P., Hervig, M.E., Siskind, D.E., Stevens, M.H., Bailey, S.M., Gumbel, J., 2014. Analysis of northern midlatitude noctilucent cloud occurrences using satellite data and modeling. J. Geophys. Res. Atmos. 119, 3238–3250. https://doi.org/10.1002/2013JD021017.

Siskind, D.E., Eckermann, S.D., McCormack, J.P., Alexander, M.J., Bacmeister, J.T., 2003. Hemispheric differences in the temperature of the summertime stratosphere and mesosphere. J. Geophys. Res. 108 https://doi.org/10.1029/2002JD002095, 4051, D2.

Siskind, D.E., Coy, L., Espy, P., 2005. Observations of stratospheric warmings and mesospheric coolings by the TIMED SABER instrument. Geophys. Res. Lett. 32, L09804. https://doi.org/10.1029/2005GL022399.

Siskind, D.E., Stevens, M.H., Hervig, M., Sassi, F., Hoppel, K., Englert, C.R., Kochenash, A.J., 2011. Consequences of recent Southern Hemisphere winter variability on polar mesospheric clouds. J. Atmos. Sol. Terr. Phys. 73, 2013–2021.

Stevens, M.H., et al., 2012. Validation of upper mesospheric and lower thermospheric temperatures measured by the Solar Occultation for Ice Experiment. J. Geophys. Res. 117, D16304. https://doi.org/10.1029/2012JD017689.

Stevens, M.H., Lieberman, R.S., Siskind, D.E., McCormack, J.P., Hervig, M.E., Englert, C. R., 2017. Periodicities of polar mesospheric clouds inferred from a meteorological analysis and forecast system. J. Geophys. Res. Atmos. 122, 4508–4527. https://doi.org/10.1002/2016JD025349.

Thurairajah, B., Cullens, C.Y., Siskind, D.E., Hervig, M.E., Bailey, S.M., 2020. The role of vertically and obliquely propagating gravity waves in influencing the polar summer mesosphere. J. Geophys. Res.: Atmospheres 125, e2020JD032495. https://doi.org/10.1029/2020JD032495.

Yuan, T., Solomon, S.C., She, C.-Y., Krueger, D.A., Liu, H.-L., 2019. The long-term trends of nocturnal mesopause temperature and altitude revealed by Na lidar observations between 1990 and 2018 at mid-latitude. J. Geophys. Res.: Atmospheres 124, 5970–5980. https://doi.org/10.1029/2018JD029828.

Zhao, X.R., Sheng, Z., Shi, H.Q., Weng, L.B., Liao, Q.X., 2020. Long-term trends and solar responses of the mesopause temperatures observed by SABER during the 2002–2019 period. J. Geophys. Res.: Atmospheres 125, e2020JD032418. https://doi.org/10.1029/2020JD032418.